Article

Not peer-reviewed version

AuAgS/rGO and MnCdO/rGO Nanocomposite-Based Sensors for Electrochemical Detection of Organophosphorus Pesticides

Saeid Masoudnia and Esmaeil Salahi *

Posted Date: 27 November 2025

doi: 10.20944/preprints202511.2092.v1

Keywords: water contamination; non-enzymatic detection; Diazinon; electrochemical sensor; reduced graphene oxide

 doi:10.20944/preprints202511.2092.v1

Article

AuAgS/rGO and MnCdO/rGO Nanocomposite-Based Sensors for Electrochemical Detection of Organophosphorus Pesticides

Saeid Masoudnia and Esmaeil Salahi *

Department of Ceramic, Materials and Energy Research Center, Karaj, Iran

* Correspondence: e-salahi@merc.ac.ir

Abstract

The use of pesticides in agriculture is essential for protecting crops and enhancing yield. However, their widespread application poses significant environmental and health risks. This study focuses on creating novel non-enzymatic electrochemical sensors for this purpose. Two nanocomposite-based sensors were developed, one using a bimetallic AuAgS alloy with reduced graphene oxide (AuAgS/rGO) and another using a MnCdO metal oxide with rGO (MnCdO/rGO). These nanomaterials were synthesized and deposited onto fluorine-doped tin oxide (FTO) electrodes. The materials were characterized using techniques such as FESEM, TEM, EDX, XRD, and UV-Vis spectroscopy. Sensor performance was evaluated using differential pulse voltammetry (DPV) for the detection of diazinon and ethion. Comprehensive characterization confirmed the successful synthesis and desired morphological properties of the nanomaterials. The AuAgS/rGO-based sensor demonstrated exceptional sensitivity, with detection limits of 6 nM/L for diazinon and 50 nM/L for ethion, and wide linear ranges of 12-500 nM/L and 120-490 nM/L, respectively. The MnCdO/rGO sensor was successfully applied to detect diazinon in a real-world sample of orange wash, confirming its practical utility. This study underscores the potential of these nanocomposite-based sensors as highly sensitive, selective, and practical tools for the precise monitoring of organophosphorus pesticides (OPPs) in environmental and food safety applications.

Keywords: water contamination; non-enzymatic detection; Diazinon; electrochemical sensor; reduced graphene oxide

1. Introduction

The growing global population has led to an increased demand for food [1]. To meet this demand, it is crucial to establish optimal conditions for the agricultural sector, enabling enhanced production with minimal risk of pollution [2]. This can be achieved through the use of high-quality fertilizers and pesticides [1]. While numerous types of pesticides have been developed, many are only partially safe and healthy. According to the Global Agriculture Land office, 64% of pesticide pollution is attributed to a single type of developed pesticide. Chemists classify pesticides based on their chemical structure, with major categories including organochlorates, organophosphorus, carbamates, pyrethroids, phenyl amides, phenoxy alkanes, triazines, benzoic acids, phthalimides, and others [3].

Diazinon and ethion are two commonly used organophosphate pesticides. They are prevalent in pest control and are frequently found in agricultural runoff, posing risks to water supplies and ecosystems [4]. Detecting organophosphorus like Diazinon and Ethion is vital due to their extensive use in agriculture, potential to cause environmental harm, and significant health risks to humans [5].

Over the past two decades, a variety of methods have been developed for the quantitative detection and qualitative determination of substances [4-7]. The sensitivity of these methods can be

 doi:10.20944/preprints202511.2092.v1

enhanced by optimizing certain parameters, such as performing pre-treatment operations [8] and selecting suitable techniques, and using the correct setup [9]. Scientists have developed electroanalytical techniques to address the detection of pesticides. Electrochemical techniques can detect pesticides that exhibit electroactive properties through oxidation and reduction reactions, which lead to the breakdown of pesticides [10]. Electrochemical and biosensors utilizing nanomaterials have been developed for pesticide detection [6], often employing enzyme-modified electrodes with enzymes such as ascorbate oxidase and tyrosinase. Both non-metallic (e.g., carbon-based) and metallic nanomaterials are extensively researched for their ability to enhance sensor performance [7]. Enzyme-based biosensors, while widely used for pesticide detection, suffer from several significant limitations primarily stemming from the inherent nature of enzymes. These biosensors are highly susceptible to environmental conditions such as pH, temperature, ionic strength, and the presence of chemicals or heavy metals, which can lead to enzyme denaturation, reduced catalytic activity, and instability over time. This results in short operational lifespans, low reproducibility, and limited practical applicability, especially in field conditions. Additionally, enzyme-based detection often relies on inhibition mechanisms that lack specificity, making it difficult to distinguish between different pesticides within the same class, such as organophosphates or carbamates. This can lead to false positives and restricts the ability to perform multiplexed detection. Furthermore, the need for careful handling, storage, and skilled personnel further complicates their use in on-site and point-of-care testing, hindering commercialization and widespread deployment [11]. The advancement of detection technologies, particularly non-enzymatic electrochemical sensors, plays a crucial role in overcoming these challenges [12]. Such sensors provide a promising solution for the rapid [13], cost-effective [14], and accurate detection of organophosphorus, ensuring food safety [15], environmental protection [16], and public health. Non-enzymatic electrochemical sensors, which utilize a synergy of noble metal sulfides (NMS) and reduced graphene oxide (rGO) [17], are emerging as pivotal technologies for efficiently detecting organophosphorus [18]. These sensors offer exceptional selectivity and sensitivity due to the catalytic capabilities of NMS and the high surface area of rGO, which enhance trace detection in complex environments such as soil and water [19]. Compared to enzyme-based sensors, non-enzymatic sensors boast cost-effectiveness and greater stability [20], as they are not prone to degradation over time, making them ideal for sustained environmental monitoring [21]. With their rapid response capabilities, these sensors provide real-time feedback essential for timely decision-making, particularly in ensuring the safety of food and water [22]. They are environmentally friendly due to the sustainable nature of rGO and are adaptable to diverse conditions [23], making them suitable for various applications. Their high sensitivity and ability to detect OPPs at low concentrations ensure compliance with regulatory standards [24]. Additionally, these sensors can be tailored to detect a wide range of organophosphorus and other hazardous chemicals [25], increasing their applicability across sectors [26]. Simple fabrication processes reduce costs and facilitate widespread deployment [27], while their potential for miniaturization enhances portability, further broadening their utility and enabling on-site and field testing with ease [28].

Previous studies on OPP detection faced significant limitations, leading to the development of sensors based on NMS and rGO [29]. The limitations include stability and selectivity issues in enzymatic sensors [30], limited sensitivity of non-enzymatic materials [31], poor selectivity in complex matrices [5], high cost and scalability challenges [6]. Enzyme-based sensors, such as those using acetylcholinesterase, suffer from poor thermal and chemical stability [32], short shelf life, and interference from other cholinesterase inhibitors like carbamates [33]. Traditional non-enzymatic materials, such as metal oxides and conducting polymers, exhibit high detection limits (LODs > 10 nM) due to slow electron transfer and low catalytic activity [31]. Co-existing ions (e.g., Cl^-, NO_3^-) and organic compounds in real samples, such as soil and food, cause poor selection due to adsorb on sensor surfaces that leads to false positives or negatives [5].

Non-enzymatic electrochemical sensors based on NMS and reduced graphene oxide rGO have emerged as highly effective tools for detecting OPPs, such as Diazinon and Ethion [34]. The motivation for the development of these sensors stems from the high toxicity of OPPs, which pose significant risks to human health [35], animal welfare [36], and the environment. These pesticides

 doi:10.20944/preprints202511.2092.v1

inhibit essential enzymes like acetylcholinesterase, leading to severe poisoning and environmental contamination [37]. The integration of NMS materials, such as gold or silver sulfide, with rGO significantly enhances the performance of these sensors. NMS facilitates electrochemical reactions, improving sensitivity, while rGO's high surface area ensures superior interaction with target pesticide molecules [38]. The high sensitivity of these sensors allows the detection of OPPs at concentrations well below regulatory limits for pesticide residues. This makes them invaluable for monitoring pesticide use in agriculture, as well as for assessing water quality and ensuring food safety [37].

In this study, we developed non-enzymatic electrochemical sensors based on AuAgS/rGO and MnCdO/rGO nanocomposites and investigated their efficiency for selective and sensitive detection of organophosphate pesticides diazinon and ethion. The performance of these sensors was comprehensively evaluated through various electrochemical and microscopic techniques, and their detection limit and linear range were compared with existing methods. We expect this novel sensing platform to provide a practical solution for environmental monitoring and food safety.

2. Materials and Methods

2.1. Materials

The following materials and equipment were used in this study: Gold Cyanide, Silver Cyanide , Sodium Sulfide (Na_2S), Reduced Graphene Oxide (rGO), Manganese Acetate ($Mn(CH_3CO_2)_2$), Cadmium Acetate ($Cd(O_2CCH_3)_2(H_2O)_2$), Ethanol, Anhydrous Propanol, Deionized Water, Tin Oxide Doped with Fluorine on Glass, Fluorine-doped Tin Oxide (FTO), Field Emission Scanning Electron Microscope (X-ray Diffraction Spectroscopy was attached to the FESEM device), UV-Vis Spectrophotometer, Transmission Electron Microscope, Electrochemical Impedance Spectroscopy (EIS), Cyclic Voltammetry (CV).

2.2. Preparation of AuAgS/rGO

In a standardized procedure, equal volumes (50 mL each) of 0.05 M (AuCN) and (AgCN) solutions were combined. Subsequently, 10 mL of a solvent mixture (ethanol:propanol, 4:1 v/v) was introduced. The mixture was stirred at 350 rpm at 5 °C. A 0.01 M Na_2S solution was added dropwise (total 75 mL) until precipitation was complete. Stirring was continued overnight. The synthesized nanoparticles were isolated by centrifugation at 4000 rpm for 20 minutes. The black precipitate was washed three times with deionized water and dried at 110 °C for 20 hours.

2.3. Fabrication of FTO by Prepared Particles

FTO substrates (1 × 2 cm) were cleaned ultrasonically in acetone and ethanol. Two distinct solutions were prepared for the deposition steps: (1) Sol A: 0.1 g of synthesized AuAgS nanoparticles was dispersed in 70% propanol, (2) Sol B: 0.03 g of rGO was dissolved in deionized water with 100 µg of potassium chloride (KCl) added as a supporting electrolyte. he cleaned FTO electrode (cathode) and a platinum wire anode (2 cm) were immersed in Sol A, Electrophoretic deposition was performed at 100 V for 20 minutes. The electrode was rinsed with DI water. Subsequently, the rGO layer was deposited from Sol B using an applied potential of 2.0 V. This electro-fabrication process was repeated three times to ensure a uniform and robust rGO coating. This multi-step deposition procedure, involving both AuAgS nanoparticles and rGO, was designed to optimize the electrochemical properties of the sensor, ensuring high stability and enhanced conductivity for the subsequent electrochemical measurements.

2.4. Diazinon and Ethion Detection

The AuAgS/rGO-modified FTO electrode was used as the working electrode. Electrochemical detection of diazinon and ethion was performed in standard solutions with concentrations of 3, 6, 12, 24, 50, 100, 200, 500, and 1000 nM/L. Techniques included CV, EIS, NPV, and DPV. A three-electrode system was used: the modified FTO working electrode, a saturated calomel reference electrode (SCE), and a platinum foil counter electrode.

 doi:10.20944/preprints202511.2092.v1

2.5. Characterization of AuAgS / rGO Nanoparticles

The synthesized AuAgS nanoparticles were characterized by UV-Vis spectrophotometry (Cecil 1021) to assess optical properties and surface plasmon resonance (SPR). Morphology and shape were analyzed by FESEM (ZEISS Sigma 500). Elemental composition was determined by EDX, and size/internal structure were investigated by TEM (JEM-2100 Plus).

2.6. Synthesis and Modification of Mn-CdO/RGO Composite Electrode

A modified electrode was developed using a MnCdO/rGO composite via a two-step process: (1) first Layer (MnCdO): Solution A was prepared with 0.05 M $MnCl_2$ and 0.05 M $CdCl_2$ in dimethyl sulfoxide (DMSO). Electrodeposition onto an FTO working electrode (vs. SCE reference and Pt counter) was carried out at -1.03 V for 20 minutes. The electrode was rinsed, dried, and thermally oxidized at 350 °C for 4 hours under oxygen. (2) Second layer (MnCdO/rGO): Solution B was prepared similarly to Solution A but with the addition of 0.01 M graphene oxide (GO). The first-layer electrode was placed in Solution B, and electrodeposition was repeated at -1.03 V for 20 minutes. The electrode was then anodized in 5% H_2O_2 at +0.8 V for 1 hour to oxidize the second layer, washed, and dried.

2.7. Diazinon Detection with MnCdO/rGO Electrode

The prepared MnCdO/rGO-FTO electrode was used as a sensor. Electrochemical tests (CV, EIS, NPV, DPV) were conducted in standard diazinon solutions (10, 25, 50, 100 ppm). A three-electrode system was used including MnCdO/rGO-FTO working electrode, SCE reference, and Pt foil counter.

2.8. Characterization of MnCdO / rGO Nanoparticles

The synthesized MnCdO nanoparticles were characterized by UV-Vis spectrophotometry. Morphology and shape were determined by FESEM, elemental analysis by EDX, and size/structure by TEM.

3. Results and Discussion

3.1. Characterization of AuAgS Nanoparticles

The UV-Vis spectrum of AuAgS nanoparticles dispersed in water:ethanol (4:1) showed an absorption onset between 350 nm and 800 nm (Figure 1). Distinct peaks were observed; a broad peak for Ag_2S at 400 nm (SPR) and a peak for AuS at 605 nm. The SPR for AuAgS nanoparticles appeared as a broad peak at 535 nm. This peak showed red and blue shifts compared to Ag_2S and Au_2S, respectively, consistent with literature studies [39, 40, 12, 20]. The single absorption peak suggests the successful formation of the AuAgS compound without detectable impurities.

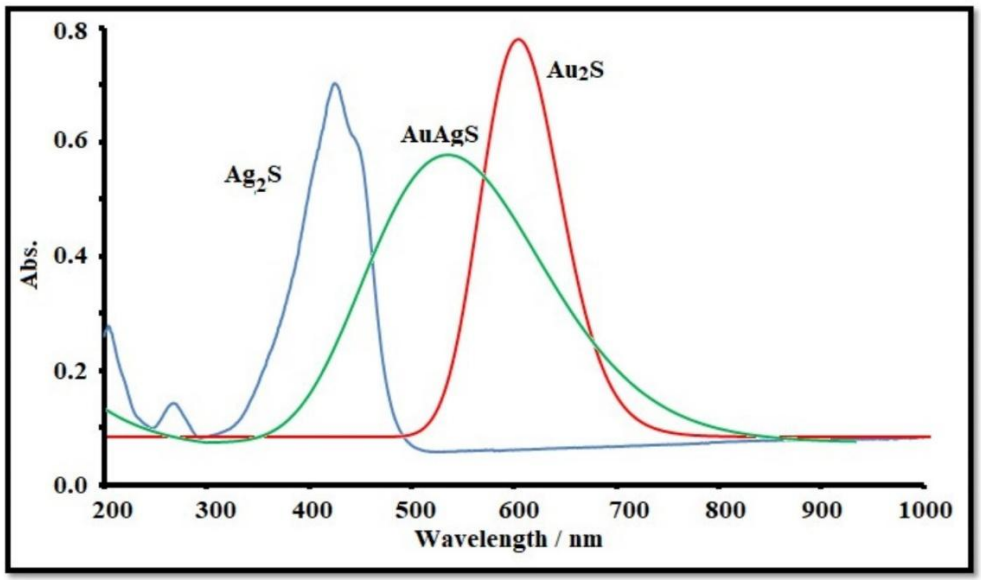

 doi:10.20944/preprints202511.2092.v1

Figure 1. UV-Visible spectra of Ag2S , Au2S and AuAgS alloy nanoparticles as a function of irradiation time.

3.2. XRD

XRD analysis confirmed the crystallographic structures (Figure 2). Peaks for Au and Ag nanoparticles matched standard JCPDS patterns (04-0783 for both), with characteristic FCC structure peaks at 2θ = 38.3°, 44.5°, 64.5°, and 77.9°, corresponding to (111), (200), (220), and (311) planes, respectively (Mohammadi et al., 2016, Wang et al., 2024). The rGO pattern showed broad peaks at 24° (002 plane) and 44° (101 plane), indicating successful reduction and monolayer formation with an average thickness of around 1 nm [10, 18]. The XRD pattern for AuAgS/rGO showed peaks corresponding to both monometallic (Ag, Au) and bimetallic sulfide structures, confirming their presence. A subtle peak shift was observed, likely due to interaction with the rGO substrate, which can alter the local electronic environment or induce strain [10, 13, 14]. This confirms the successful synthesis of the AuAgS-rGO composite. According to the previous studies that demonstrated rGO makes the sensors preferable for applications. Additionally, the potential for simple fabrication and miniaturization ensures wide scalability and accessibility, even in resource-constrained settings, highlighting their advantage over more complex and less versatile alternatives [41]. The high surface area of rGO (2630 m^2/g) and conductivity (10^3 S/cm) enhance electron transport, while NMSs lower the overpotentials for OPP oxidation. Density functional theory (DFT) studies confirm that AuS-rGO interfaces reduce the energy barrier for diazinon oxidation by 0.3 eV compared to pure gold [42]. The XRD analysis of Au, Ag, and AuAgS nanoparticles impregnated with rGO reveals important structural insights. The typical FCC crystalline structures of Au and Ag NPs were confirmed, and the distinctive features of rGO were also observed. The bimetallic AuAgS nanoparticles, when impregnated with rGO, exhibited shifts in the diffraction patterns, suggesting a strong interaction between the metal sulfides and the rGO substrate. These findings provide valuable information regarding the crystallinity, composition, and the interfacial interactions in these composite materials, which are crucial for their performance in various applications, including catalysis, sensing, and energy storage.

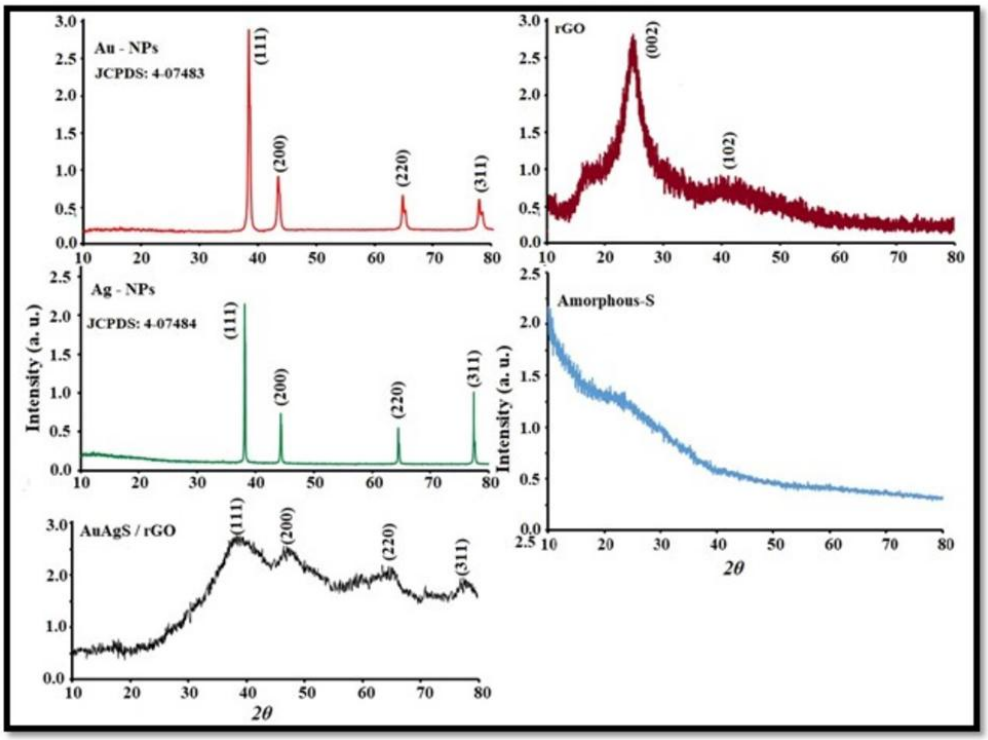

Figure 2. XRD spectrum of NPs of Au, Ag and AuAgS, and spectrum of nano-sheet of rGO and Amorphous Sulphur particles.

3.3. TEM and FESEM/EDX studies

 doi:10.20944/preprints202511.2092.v1

3.3.1. TEM and FESEM/EDX Analysis of AuAgS/rGO Nanoparticles

TEM analysis: TEM images (Figure 3) revealed spherical AuAgS nanoparticles with an average diameter of approximately 15 nm, indicating successful synthesis.

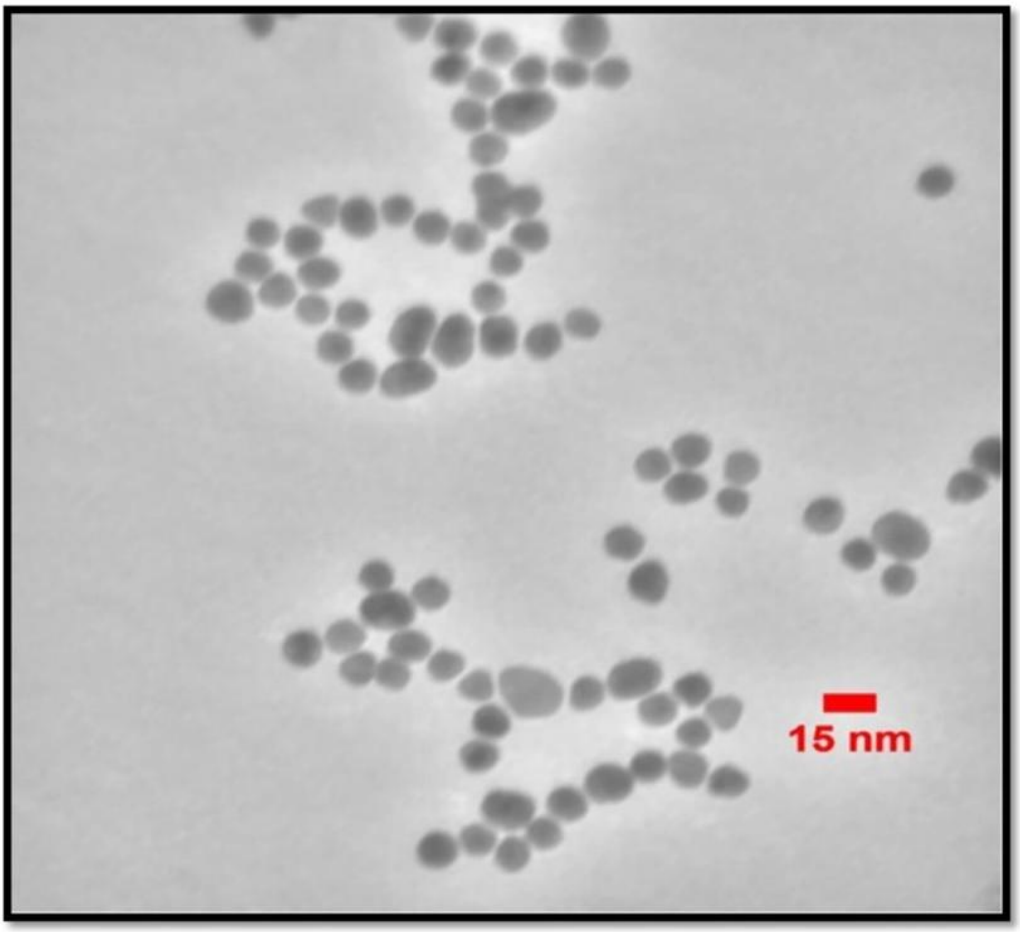

Figure 3. Representative TEM image of synthesized AuAgS nanoparticles.

Electrophoretic coating on FTO glass: FESEM images (Figure 4) showed the electrophoretic coating of AuAgS/rGO nanoparticles on FTO glass, depicting a uniform coating with some agglomeration.

Energy-Dispersive X-Ray Spectroscopy (EDX) spectrum analysis: The EDX spectrum (Figure 4) confirmed the presence of Au (53.1%), Ag (28.8%), S (8.4%), C (3.9%), and O (5.32%). Based on mass and atomic percentages, the composition index *x* in $Au_xAg_xS_x$/rGO was approximately 1, indicating a balanced stoichiometry. The EDX spectrum revealed the presence of key elements including gold (Au), silver (Ag), sulfur (S), carbon ©, and oxygen (O) with precents 53.1, 28.8, 8.4, 3.9 and 5.32, respectively. These elements are essential components of the AuAgS/rGO nanocomposite.

 doi:10.20944/preprints202511.2092.v1

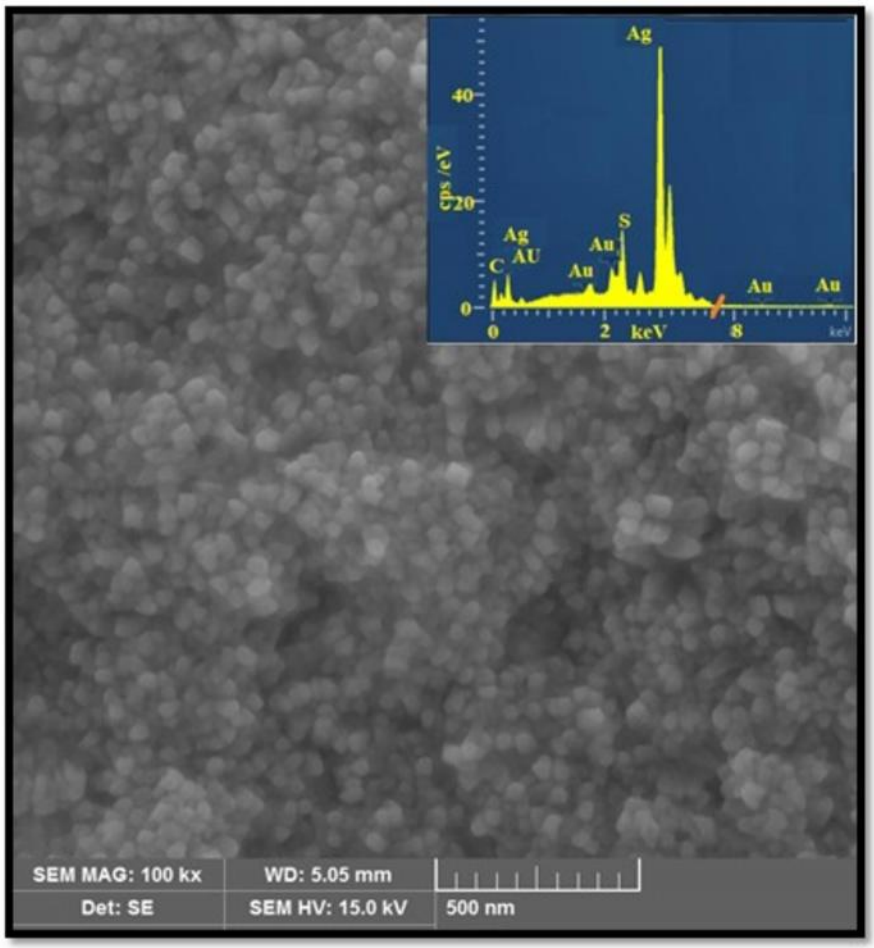

Figure 4. Morphological studies of AuAgS/rGO coated layer by FESEM and elemental analysis of fabricated layer by EDX spectrum.

3.4. Electrochemical Detection of Organophosphate Pesticides

The electrochemical sensitivity of the AuAgS/rGO-FTO electrode for diazinon and ethion was assessed using EIS, CV, NPV, and DPV in a 0.001 M diazinon solution. DPV exhibited the highest sensitivity. Figure 5 presents DPV curves for diazinon and ethion at concentrations of 3, 6, and 12 nM/L. Detection of diazinon was more precise than for ethion, suggesting different interaction dynamics.

3.5. DPV Technique: Sensitivity and Linearity

Figure 5 illustrates DPV curves for various concentrations of diazinon and ethion. DPV offers superior sensitivity by minimizing background current.

 doi:10.20944/preprints202511.2092.v1

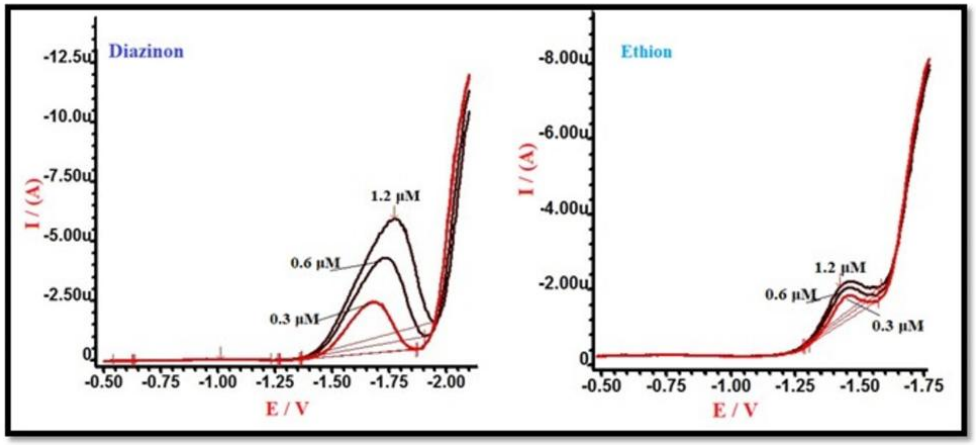

Figure 5. DPV response of the fabricated electrode AuAgS/rGO for Diazinon and Ethion in the standard solutions (0.3, 0.6 and 1.2 µM).

Limit of Detection (LOD): The LOD was 6 nM/L for diazinon and 50 nM/L for ethion, indicating high sensitivity for trace-level detection.

Linearity Range: The linearity range was 12–500 nM/L for diazinon and 120–490 nM/L for ethion (Figures 6 and 7), providing a robust window for quantification.

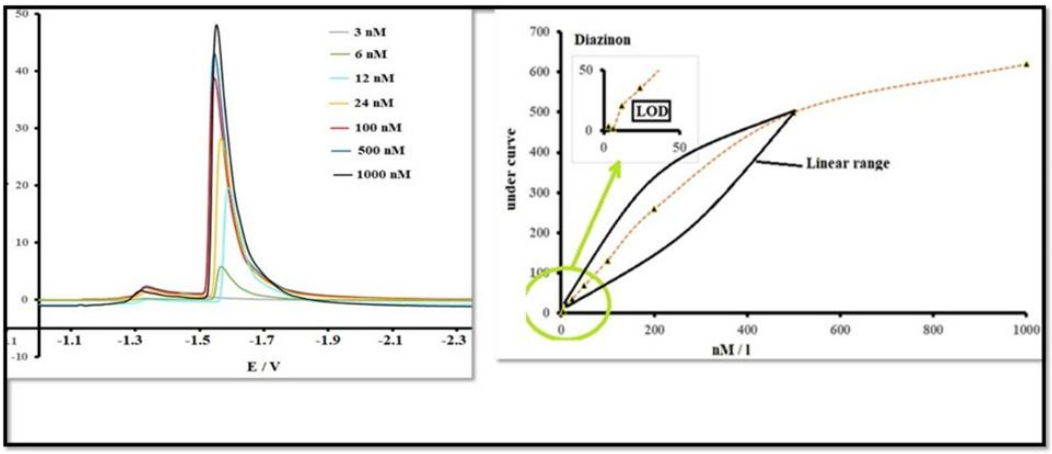

Figure 6. DPV response of the fabricated electrode AuAgS/rGO for Diazinon and response curve to find LOD and linear range of Electrode to different concentration of Diazinon.

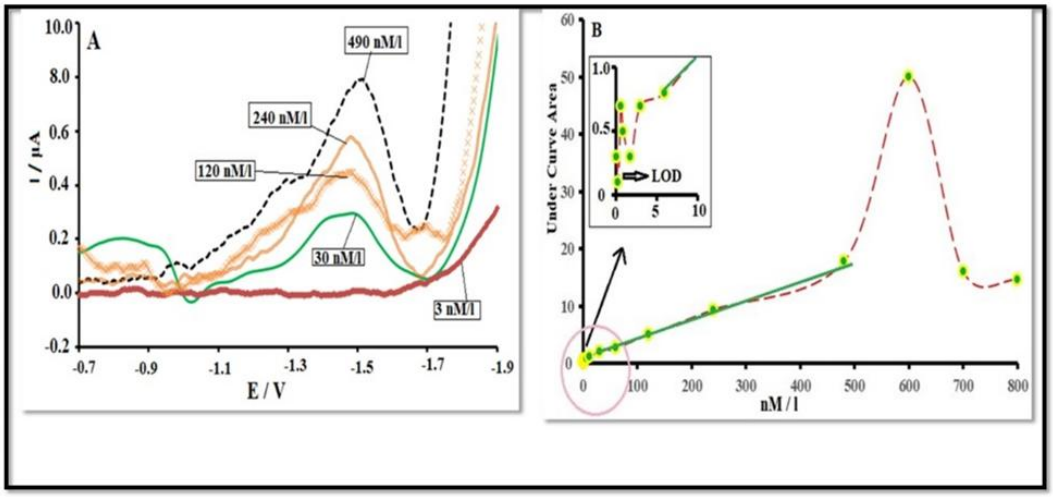

Figure 7. DPV response of the fabricated electrode AuAgS/rGO for ethion and response curve to find LOD and linear range of Electrode to different concentration of Ethion.

 doi:10.20944/preprints202511.2092.v1

3.6. Advantages of DPV

DPV offers higher sensitivity, a wider linearity range, and a lower LOD compared to other techniques due to its differential pulse mechanism minimizing background noise. The detection of diazinon and ethion using DPV has been the subject of considerable research. Previous studies have investigated and compared electrochemical sensors used for the detection of diazinon [15, 17, 26].

3.7. Comparative Performance

The AuAgS/rGO-FTO electrode detected diazinon at concentrations as low as 3 nM. Reducing the working electrode surface area to 0.3 cm^2 shifted the linearity range from 6 nM to 2 µM for Diazinon, suggesting that optimization of electrode geometry can enhance performance.For ethion, DPV curves at 3, 30, 120, 240, and 490 nM/L confirmed its electroactive nature (Figure 7). The linear range was 120–490 nM/L, comparable to that for diazinon with the same electrode. The LOD for Ethion was 50 nM/L, indicating the electrode's promising potential for quantifying both pesticides. The noise and fluctuations observed in the DPV curves are typical for an electrode in its initial state, which may be attributed to the surface roughness or imperfections. However, these fluctuations could potentially be minimized through further modification of the electrode structure, leading to smoother and more stable curves. This would enhance the electrode's overall performance and sensitivity. The linear concentration ranges and low LOD values demonstrate its capability for precise pesticide detection in environmental monitoring applications. In comparison to other sensors, the LOD of AuAgS/rGO-FTO for Diazinon was fewer (Table 1) that confirms the efficiency of the electrode. Sensors found for Ethion and their LOD are shown in Table 2. In comparison to other sensors, The LOD of AuAgS/rGO-FTO for Ethion was fewer than LOD of DNA-templated Silver Nanoclusters (DNA-Ag NCs) (LOD: 30 ng/ml= 78.03 nM/L) and multi-walled carbon nanotube–polyvinyl chloride (MWNT–PVC) (LOD: 30 ng/ml= 57.22 nM/L) [45, 47], but was mor than the LOD of Silver Nanoparticles (AgNPs) (LOD: 3.7 ng/ml= 9.62 nM/L) [46]. The molecular weight of Ethion is 384.48 g/mol [48]. The next steps could involve improving electrode modifications to reduce noise and enhance overall sensitivity for both pesticides [15, 17, 18, 20].

Table 1. Comparison LOD of AuAgS/rGO-FTO and other sensors for the detection of Diazinon.

Sensor Type	Recognition Element	Detection Method	LOD	Reference
Impedimetric Biosensor	Lipase from Candida Rugosa (CRL)	EIS	10 Nm/L	43
Impedimetric Biosensor	Lipase from Porcine Pancreas (PPL)	EIS	0.1 µM/L	43
Aptamer-based Fluorescent Biosensor	ssDNA Aptamer (DIAZ-02, DIAZ-03)	Fluorescence	148 Nm/L (stated as ppb level)	44

Table 2. Comparison LOD of AuAgS/rGO-FTO and other sensors for the detection of Ethion.

Sensor Type	Recognition Element	Detection Method	LOD	Reference

 doi:10.20944/preprints202511.2092.v1

Fluorescence Biosensor	DNA-templated Silver Nanoclusters (DNA-Ag NCs)	Fluorescence Quenching	30 ng/mL	45
Resonance Rayleigh Scattering (RRS) Sensor	Silver Nanoparticles (AgNPs)	Resonance Rayleigh Scattering Quenching	3.7 µg/L (which is ~3.7 ng/mL)	46
Screen-Printed Potentiometric Sensor	multi-walled carbon nanotube–polyvinyl chloride (MWNT–PVC)	Butyrylcholinesterase enzyme inhibition by Ethion	22.0 ng/mL	47
Sensor Type	**Recognition Element**	**Detection Method**	**LOD**	**Reference**
Fluorescence Biosensor	DNA-templated Silver Nanoclusters (DNA-Ag NCs)	Fluorescence Quenching	30 ng/mL	45
Resonance Rayleigh Scattering (RRS) Sensor	Silver Nanoparticles (AgNPs)	Resonance Rayleigh Scattering Quenching	3.7 µg/L (which is ~3.7 ng/mL)	46
Screen-Printed Potentiometric Sensor	multi-walled carbon nanotube–polyvinyl chloride (MWNT–PVC)	Butyrylcholinesterase enzyme inhibition by Ethion	22.0 ng/mL	47

3.8. Characterization and Performance of MnCdO/rGO Sensor

FESEM images of the MnCdO/rGO coated layer at different magnifications (Figure 8 A: 1 µm scale, B: 200 nm scale) show a well-defined hierarchical hybrid structure. MnCdO nanoparticles (40–80 nm) were uniformly distributed on rGO sheets, creating a porous, multi-scaled morphology. The EDX spectrum (Figure 8A) confirmed the presence of Mn, Cd, O, C, Au, Ag, and S, indicating successful composite formation. The uniform elemental distribution and absence of impurity peaks reflect homogeneous incorporation.

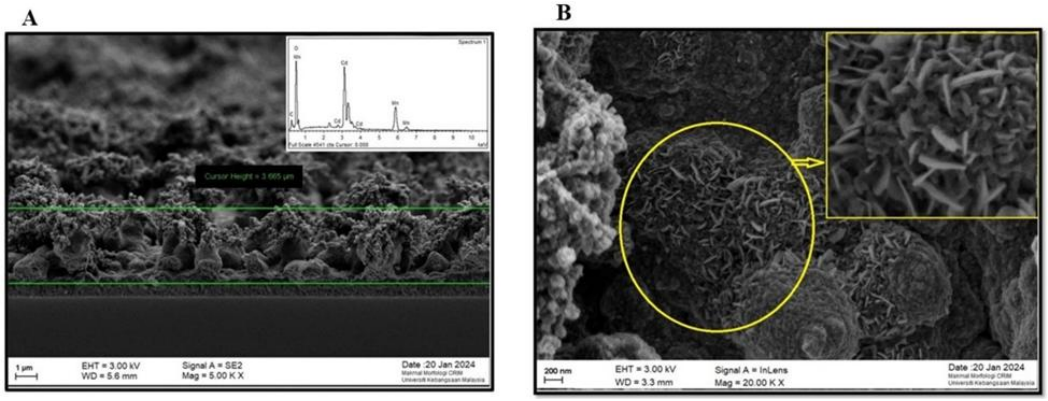

 doi:10.20944/preprints202511.2092.v1

Figure 8. The morphological studies and elemental analysis of the MnCdO/rGO coated layer. (A) FESEM on scale 1 μm and the elemental analysis of the fabricated layer using EDX . (B) FESEM n scale 200 nm.

XRD analysis (Figure 9) identified graphene oxide (GO) (002 and 100 peaks), manganese oxide (MnO) (101, 006, 119, 301 peaks), and cadmium oxide (CdO) (111, 200, 220, 311, 222 peaks) phases. The intense CdO (220) peak suggests it is the most abundant phase. Broader peaks indicate nanoscale crystallites. The absence of unexpected peaks confirms clean synthesis.

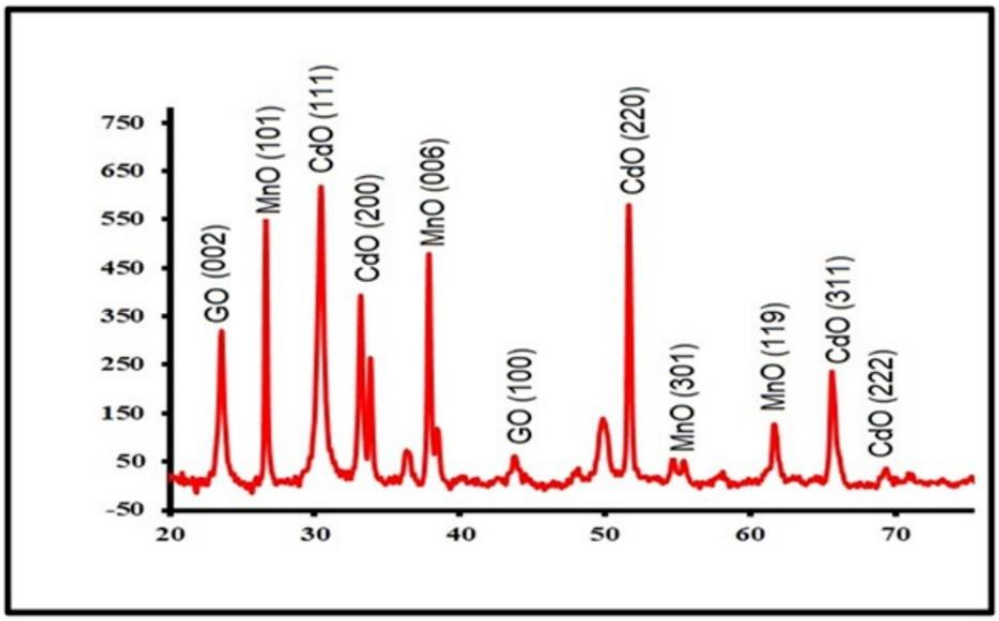

Figure 9. The XRD (X-ray Diffraction) patterns for (a) Au nanoparticles, (b) Ag nanoparticles, © AuAgS/rGO, (d) rGO, and (e) amorphous sulfur particles.

3.9. DPV Detection of Diazinon with MnCdO/rGO Electrode

Figure 10 shows DPV measurements for diazinon detection using the MnCdO/rGO electrode. Curves are shown for a blank solution and diazinon concentrations of 10, 25, and 100 ppm. The peak current increases with concentration. A sample from an orange wash was analyzed, and its DPV peak overlapped with the standard 50 ppm curve, indicating a diazinon concentration of approximately 50 ppm in the sample.

 doi:10.20944/preprints202511.2092.v1

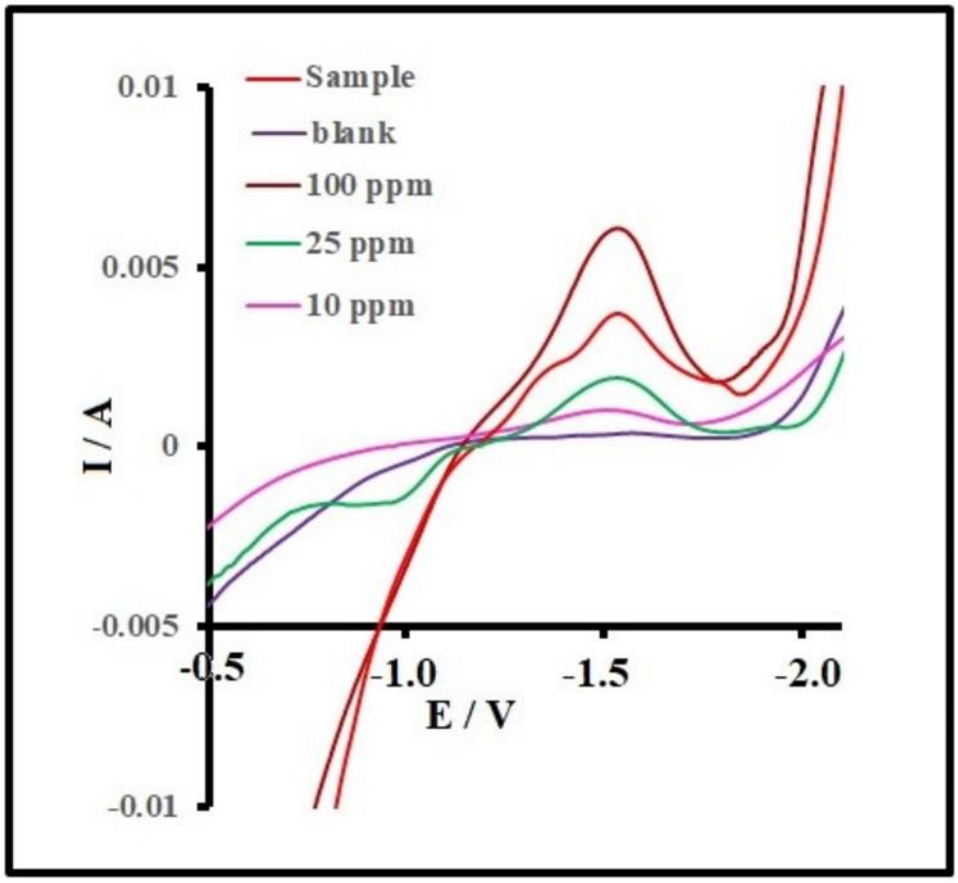

Figure 10. The results of DPV measurements performed with the MnCdO/rGO electrode for diazinon detection.

3.10. Limit of Detection (LOD) and Linear Range

The MnCdO/rGO electrode showed a strong electrochemical response to diazinon, with linear behavior within a specific concentration range, making it suitable for real-world applications.

4. Conclusions

Pesticide residues pose significant risks to human health and environmental sustainability. This study developed novel non-enzymatic electrochemical sensors based on AuAgS/rGO and MnCdO/rGO nanocomposites for detecting OPPs like diazinon and ethion. Comprehensive characterization confirmed the successful synthesis and desired properties of the nanomaterials. Among the electrochemical techniques evaluated, DPV proved most effective, demonstrating high sensitivity with low detection limits (6 nM/L for diazinon, 50 nM/L for ethion) and wide linear ranges. The successful application of the MnCdO/rGO sensor to detect diazinon in a real orange wash sample highlights its practical utility. These sensors offer advantages of high sensitivity, selectivity, cost-effectiveness, rapid detection, and portability, making them ideal for on-site monitoring in environmental and food safety applications. Future work should focus on expanding selectivity profiling, exploring cost-effective materials, optimizing sensor design for field use, and further validation in complex real-world matrices.

Author Contributions: SM: Conceptualization, Data curation, Formal analysis, Investigation, Methodology, Software, Validation, Writing – original draft. ES: Supervision, Conceptualization, Project administration, Resource, Data curation, Formal analysis.

Funding: This work was supported by the Materials and Energy Research Center, Karaj, Iran (grant NO: 311402005).

Institutional Review Board Statement: Not applicable.

 doi:10.20944/preprints202511.2092.v1

Data availability: All data and materials are included in the manuscript.

Conflicts of Interest: The authors declare no conflicts of interest.

Abbreviations

The following abbreviations are used in this manuscript:

Rgo	reduced graphene oxide
DPV	Differential pulse voltammetry
FTO	Fluorine-doped tin oxide
OPPs	Organophosphorus pesticides
NMS	Noble metal sulfides
Na_2S	Sodium Sulfide
FESEM	Field Emission Scanning Electron Microscope
XRD	X-ray Diffraction
TEM	Transmission Electron Microscope
CV	Cyclic Voltammetry
EIS	Electrochemical Impedance Spectroscopy
KCl	Potassium chloride
SCE	Saturated calomel reference electrode
SPR	Surface plasmon resonance
DMSO	Dimethyl sulfoxide
DFT	Density functional theory
EDX	Energy-Dispersive X-Ray Spectroscopy
LOD	Limit of Detection

References

1. Jayaraj, R.; Megha, P.; Sreedev, P. Organochlorine pesticides, their toxic effects on living organisms and their fate in the environment. Interdiscip. Toxicol. 2016, 9, 90–100.
2. Ravikumar, C.H.; Lavanya, C.; Akash, S.; Shwetharani, R.; Surareungcahi, W.; Balakrishna, R.G. Nanomaterials for organophosphate sensing: present and future perspective. In: Sensing of Deadly Toxic Chemical Warfare Agents, Nerve Agent Simulants, and their Toxicological Aspects. Elsevier, 2023, pp. 183-202.
3. Pathiraja, G.; Bonner, C.D.; Obare, S.O. Recent advances of enzyme-free electrochemical sensors for flexible electronics in the detection of organophosphorus compounds: a review. Sensors. 2023, 23, 1226.
4. Radi, A.E.; Oreba, R.; Elshafey, R. Molecularly imprinted electrochemical sensor for the detection of organophosphorus pesticide profenofos. Electroanalysis. 2021, 33, 1945–1951.
5. Ranveer, S.A.; Harshitha, C.; Dasriya, V.; Tehri, N.; Kumar, N.; Raghu, H. Assessment of developed paper strip-based sensor with pesticide residues in different dairy environmental samples. Curr. Res. Food Sci. 2023, 6, 100416.
6. Aghris, S.; Alaoui, O.T.; Laghrib, F.; Farahi, A.; Bakasse, M.; Saqrane, S.; Lahrich, S.; El Mhammedi, M. Extraction and determination of flubendiamide insecticide in food samples: A review. Curr. Res. Food Sci. 2022, 5, 401-413.
7. Rosello-Marquez, G.; Fernández-Domene, R.M.; Garcia-Anton, J. Organophosphorus pesticides (chlorfenvinphos, phosmet and fenamiphos) photoelectrodegradation by using WO3 nanostructures as photoanode. J. Electroanal. Chem. 2021, 894, 115366.
8. Wu, J.; Yang, Q.; Li, Q.; Li, H.; Li, F. Two-dimensional MnO2 nanozyme-mediated homogeneous electrochemical detection of organophosphate pesticides without the interference of H2O2 and color. Anal. Chem. 2021, 93, 4084-4091.
9. Zhang, Y.; Kang, T.F.; Wan, Y.W.; Chen, S.Y. Gold nanoparticles-carbon nanotubes modified sensor for electrochemical determination of organophosphate pesticides. Microchim. Acta. 2009, 165, 307-311.
10. Kang, M.H.; Kim, S.H.; Jang, S.; Lim, J.E.; Chang, H.; Kong, K.-j.; Myung, S.; Park, J.K. Synthesis of silver sulfide nanoparticles and their photodetector applications. RSC Adv. 2018, 8, 28447–28452.

 doi:10.20944/preprints202511.2092.v1

11. Majdinasab, M.; Daneshi, M.; Marty, J. L. Recent developments in non-enzymatic (bio) sensors for detection of pesticide residues: Focusing on antibody, aptamer and molecularly imprinted polymer. Talanta. 2021, 232, 122397.
12. Wang, L.; Gu, C.; Wu, L.; Tan, W.; Shang, Z.; Tian, Y.; Ma, J. Recent advances in carbon dots for electrochemical sensing and biosensing: a systematic review. Microchem. J. 2024, 111687.
13. Shen, Y.; Zhao, S.; Lv, Y.; Chen, F.; Fu, L. Acid red dyes and the role of electrochemical sensors in their determination. Microchem. J. 2024, 111705.
14. Liu, Y.; Ma, Y.; Zhou, J.; Li, X.; Xie, S.; Tan, R. Sythesis, Modification, and Biosensing Characteristics of Au2S/AuAgS-Coated Gold Nanorods. J. Nanomater. 2015, 2015, 530631.
15. Lohrasbi Nejad, A. Electrochemical strategies for detection of diazinon. J. Electrochem. Sci. Eng. 2022, 12, 1041–1059.
16. Guo, W.; Engelman, B.J.; Haywood, T.L.; Blok, N.B.; Beaudoin, D.S.; Obare, S.O. Dual fluorescence and electrochemical detection of the organophosphorus pesticides—ethion, malathion and fenthion. Talanta. 2011, 87, 276–283.
17. Gao, N.; Tan, R.; Cai, Z.; Zhao, H.; Chang, G.; He, Y. A novel electrochemical sensor via Zr-based metal organic framework–graphene for pesticide detection. J. Mater. Sci. 2021, 56, 19060–19074.
18. Ibáñez, D.; González-García, M.B.; Hernández-Santos, D.; Fanjul-Bolado, P. Detection of dithiocarbamate, chloronicotinyl and organophosphate pesticides by electrochemical activation of SERS features of screen-printed electrodes. Spectrochim. Acta A Mol. Biomol. Spectrosc. 2021, 248, 119174.
19. Hossain, M.I.; Hasnat, M.A. Recent advancements in non-enzymatic electrochemical sensor development for the detection of organophosphorus pesticides in food and environment. Heliyon. 2023, 9(9), e19299.
20. Dube, A., Malode, S.J., Alshehri, M.A. & Shetti, N.P. Recent advances in the development of electrochemical sensors for detecting pesticides. J. Ind. Eng. Chem. 2024, 144, 77-99.
21. Jiang, X.; Li, D.; Xu, X.; Ying, Y.; Li, Y.; Ye, Z.; Wang, J. Immunosensors for detection of pesticide residues. Biosens. Bioelectron. 2008, 23, 1577–1587.
22. Ge, L.; Li, S.-P.; Lisak, G. Advanced sensing technologies of phenolic compounds for pharmaceutical and biomedical analysis. J. Pharm. Biomed. Anal. 2020, 179, 112913.
23. Abedeen, M.Z.; Sharma, M.; Kushwaha, H.S.; Gupta, R. Sensitive enzyme-free electrochemical sensors for the detection of pesticide residues in food and water. TrAC Trend. Anal. Chem. 2024, 176, 117729.
24. Batvani, N., Alimohammadi, S. & Kiani, M.A. Nonenzymatic glucose sensor design based on carbon fiber ultra-microelectrode: Controlled with a manual micro adjuster. Anal. Chim. Acta. 2022, 1209, 339845.
25. He, J.; Xu, X.; Li, M.; Zhou, S.; Zhou, W. Recent advances in perovskite oxides for non-enzymatic electrochemical sensors: A review. Anal. Chim. Acta. 2023, 1251, 341007.
26. Scognamiglio, V.; Arduini, F.; Palleschi, G.; Rea, G. Biosensing technology for sustainable food safety. TrAC Trend. Anal. Chem. 2014, 62, 1–10.
27. Wang, S.; Zhao, J.; Ding, X.; Zhao, R.; Huang, T.; Lan, L.; Nasry, A.A.N.B.; Liu, S. Effect of starvation time on NO and N2O production during heterotrophic denitrification with nitrite and glucose shock loading. Process Biochem. 2019, 86, 108–116.
28. Wen, T.; Wang, M.; Luo, M.; Yu, N.; Xiong, H.; Peng, H. A nanowell-based molecularly imprinted electrochemical sensor for highly sensitive and selective detection of 17β-estradiol in food samples. Food Chem. 2019, 297, 124968.
29. Geto, A.; Noori, J.S.; Mortensen, J.; Svendsen, W.E.; Dimaki, M. Electrochemical determination of bentazone using simple screen-printed carbon electrodes. Environ. Int. 2019, 129, 400–407.
30. Sharma, M.; Taneja, P.; Yadav, L.; Sharma, P.; Janu, V.C.; Gupta, R. Current insights into the implementation of electrochemical sensors for comprehensive detection and analysis of radionuclides. TrAC Trend. Anal. Chem. 2024, 117845.
31. Rao, H.; Zhao, X.; Liu, X.; Zhong, J.; Zhang, Z.; Zou, P.; Jiang, Y.; Wang, X.; Wang, Y. A novel molecularly imprinted electrochemical sensor based on graphene quantum dots coated on hollow nickel nanospheres with high sensitivity and selectivity for the rapid determination of bisphenol S. Biosens. Bioelectron. 2018, 100, 341–347.
32. Yan, X.; Li, H.; Su,X. Review of optical sensors for pesticides. TrAC, Trends anal. chem. 2018, 103, 1-20.

 doi:10.20944/preprints202511.2092.v1

33. Tang, J.; Chen, W.; Ju, H. Rapid detection of pesticide residues using a silver nanoparticles coated glass bead as nonplanar substrate for SERS sensing. Sens. Actuators B Chem. 2019, 287, 576–583.
34. Gui, R.; Jin, H.; Guo, H.; Wang, Z. Recent advances and future prospects in molecularly imprinted polymers-based electrochemical biosensors. Biosens. Bioelectron. 2018, 100, 56–70.
35. Fang, L.; Jia, M.; Zhao, H.; Kang, L.; Shi, L.; Zhou, L.; Kong, W. Molecularly imprinted polymer-based optical sensors for pesticides in foods: Recent advances and future trends. Trend. Food Sci. Technol. 2021, 116, 387-404.
36. Rahimnejad, M.A; bdulkareem, R.A.; Najafpour, G. Determination of Diazinon in fruit samples using electrochemical sensor based on carbon nanotubes modified carbon paste electrode. Biocatal. Agric. Biotechnol. 2019, 20, 101245.
37. Cui, D.; Su, L.; Li, H.; Li, M.; Li, C.; Xu, S.; Qian, L.; Yang, B. Non-enzymatic glucose sensor based on micro-/nanostructured Cu/Ni deposited on graphene sheets. J. Electroanal. Chem. 2019, 838, 154–162.
38. Miglione, A.; Raucci, A.; Mancini, M.; Gioia, V.; Frugis, A.; Cinti, S. An electrochemical biosensor for on-glove application: Organophosphorus pesticide detection directly on fruit peels. Talanta. 2025, 283, 127093.
39. Khan, G.A.; Demirtaş, O.Ö.; Bek, A.; Bhatti, A.S.; Ahmed, W. Facile fabrication of Au-Ag alloy nanoparticles on filter paper: Application in SERS based swab detection and multiplexing. Vib. Spectrosc. 2022, 120, 103359.
40. Mohammadi, M.; Sepehrizadeh, Z.; Ebrahim-Habibi, A.; Shahverdi, A.R.; Faramarzi, M.A.; Setayesh, N. Enhancing activity and thermostability of lipase A from Serratia marcescens by site-directed mutagenesis. Enzyme Microb. Technol. 2016, 93, 18–28.
41. Kanoun, O.; Lazarević-Pašti, T.; Pašti, I.; Nasraoui, S.; Talbi, M.; Brahem, A.; Adiraju, A.; Sheremet, E.; Rodriguez, R.D.; Ben Ali, M. A review of nanocomposite-modified electrochemical sensors for water quality monitoring. Sensors, 2021, 21, 4131.
42. Kumaran, A.; Vashishth, R.; Singh, S.; Surendran, U.; James, A.; Chellam, P.V. Biosensors for detection of organophosphate pesticides: Current technologies and future directives. Microchem. J. 2022, 178, 107420.
43. Zehani و N.; Dzyadevych, S.V.; Kherrat, R.; Jaffrezic-Renault, N.J. Sensitive impedimetric biosensor for direct detection of diazinon based on lipases. Front. Chem. 2014, 2, 44.
44. Can, M.H.; Kadam, U.S.; Trinh, K.H.; Cho, Y.; Lee, H.; Kim, Y.; Kim, S.; Kang, C.H.; Kim, S.H.; Chung, W.S.; Lee, S.Y. Engineering novel aptameric fluorescent biosensors for analysis of the neurotoxic environmental contaminant insecticide diazinon from real vegetable and fruit samples. Front. Biosci.-Landmark. 2022, 27(3), 92.
45. Li, G.; Huang, X.; Peng, C.; Sun F. Highly sensitive fluorescence detection of three organophosphorus pesticides based on highly bright DNA-templated silver nanoclusters. Biosensors, 2023, 13(5), 520.
46. Parham, H.; Saeed, S. Resonance Rayleigh scattering method for determination of ethion using silver nanoparticles as probe. Talanta. 2015, 131, 570-6.
47. Khaled, E.; Kamel, M.S.; Hassan, H.N.; Abdel-Gawad, H.; Aboul-Enein, H.Y. Performance of a portable biosensor for the analysis of ethion residues. Talanta 2014, 119, 467-472.
48. Pohanish, R.P, Sittig's handbook of pesticides and agricultural chemicals, 2nd ed.; William Andrew: Norwich, NY, USA, 2014; 332-382.